crystals

MDPI

Article

Gyrotactic Motile Microorganisms Impact on Pseudoplastic Nanofluid Flow over a Moving Riga Surface with Exponential Heat Flux

Hassan Waqas [1], Mowffaq Oreijah [2], Kamel Guedri [2,3], Sami Ullah Khan [4], Song Yang [1], Sumeira Yasmin [5], Muhammad Ijaz Khan [6,7,*], Omar T. Bafakeeh [8], El Sayed Mohamed Tag-ElDin [9] and Ahmed M. Galal [10,11]

1 School of Energy and Power Engineering, Jiangsu University, Zhenjiang 212013, China
2 Mechanical Engineering Department, College of Engineering and Islamic Architecture, Umm Al-Qura University, Makkah 21955, Saudi Arabia
3 Research Unity, Materials, Energy and Renewable Energies, Faculty of Science of Gafsa, University of Gafsa, Gafsa 2100, Tunisia
4 Department of Mathematics, COMSATS University Islamabad, Sahiwal 57000, Pakistan
5 Department of Mathematics, Government College University Faisalabad, Faisalabad 38000, Pakistan
6 Department of Mathematics and Statistics, Riphah International University, Sector I-14, Islamabad 44000, Pakistan
7 Department of Mechanical Engineering, Lebanese American University, Beirut 1102 2801, Lebanon
8 Department of Industrial Engineering, Jazan University, Jazan 82822, Saudi Arabia
9 Faculty of Engineering and Technology, Future University in Egypt, New Cairo 11835, Egypt
10 Mechanical Engineering Department, College of Engineering, Prince Sattam Bin Abdulaziz University, Wadi Addawaser 11991, Saudi Arabia
11 Production Engineering and Mechanical Design Department, Faculty of Engineering, Mansoura University, Mansoura 35516, Egypt
* Correspondence: mikhan@math.qau.edu.pk

Abstract: ***Background:*** The improvement of the thermal conductivity of nanofluids is practical for different processes such as drug delivery, manufacturing of crystals, polymer processing, food and drink, cancer treatment, oil and gas, paper making and for many more. The bioconvection phenomenon has engrossed the attention of numerous researchers for its many applications in biotechnology, mechanical and electrical engineering. Bioconvection nanofluids are more prominent in the fields of biomedicine, pharmacy, nanodrug delivery, biomedical, automotive cooling and the military. ***Purpose:*** The major purpose of the current work was to determine the numerical and statistical analysis of a novel thermal radiation and exponential space-based heat source on the bioconvective flow of a pseudoplastic 3D nanofluid past a bidirectional stretched Riga surface. The behavior of the Arrhenius activation energy (AAE) and thermal radiation are also disclosed. ***Methodology:*** Suitable similarity transformations were used to transmute the partial differential equations of the flow-modeled phenomena into the structure of ordinary differential ones. The numerical solutions for the renewed set of ODEs were tackled by the bvp4c shooting algorithm built-in MATLAB software. Furthermore, the statistical analysis was computed by applying response surface methodology (RSM). ***Research implications:*** The numerical analysis is valid for the incompressible three-dimensional, magnetized flow of a pseudoplastic bioconvection nanofluid through a bidirectional surface with Riga plate aspects in the occurrence of activation energy. ***Social implications:*** The flow across three dimensions has quite important implementations in various fields, for example, polymer production, material production technology, the manufacturing of nano-biopolymer computer graphics, industry, powered engineering, aeroplane configurations, etc. The current analysis is more applicable in nanotechnology. ***Results:*** The consequences of flow control parameters over flow profiles were studied and explained under the graphic structures. Numerical outcomes were computed and discussed in detail. From the results, it was noted that the velocity field was increased via a larger mixed convection parameter. The temperature distribution was boosted via the thermal Biot number. The concentration of nanoparticles declined via the greater Lewis number. Furthermore, the motile microorganisms field was reduced via the Peclet number. ***Originality:*** Until now, no investigation has been recognized to examine the consequences of the bioconvection flow of three-dimensional pseudoplastic nanofluids

Citation: Waqas, H.; Oreijah, M.; Guedri, K.; Khan, S.U.; Yang, S.; Yasmin, S.; Khan, M.I.; Bafakeeh, O.T.; Tag-ElDin, E.S.M.; Galal, A.M. Gyrotactic Motile Microorganisms Impact on Pseudoplastic Nanofluid Flow over a Moving Riga Surface with Exponential Heat Flux. *Crystals* **2022**, *12*, 1308. https://doi.org/10.3390/cryst12091308

Academic Editors: Borislav Angelov, Sławomir Grabowski and Charles Rosenblatt

Received: 23 July 2022
Accepted: 9 September 2022
Published: 16 September 2022

past a Riga plate containing motile microorganisms utilizing the shooting method called bvp4c. ***Conclusions:*** From the results, it was concluded that nanofluids are more helpful for heat transfer increments. Furthermore, from the experimental design observed, the response declined via the thermophoresis parameter, which was significant from the ANOVA observed model.

Keywords: pseudoplastic; nanofluid; gyrotactic motile microorganism; exponential space-based heat source; activation energy; shooting scheme

1. Introduction

Fluid dynamics is important in several manufacturing applications, including chemical engineering, medical and biological fields, and in innovative technologies, particularly nanotechnology. Various investigators are trying to identify the stability of fluid dynamics in a wide range of useful applications in order to effectively recognize its rheological behavior. Scientists and researchers cited the non-Newtonian flow of fluids as a major motivation for their investigation. Several manufacturing fluids, such as specific fuels, paper ingredients, paints, beauty products, slurries, oils, as well as the melting of polycrystals, have flow with non-Newtonian fluid characteristics. It is well understood that a particular fluid representation cannot articulate all of the properties of all non-Newtonian fluid flow. Several earlier recommendations from the literature have discovered that non-Newtonian fluids can be defined by employing a variety of fundamental expressions. Numerous fluid models have been established to explore pseudoplastic fluids (shear thinning), such as the Ellis model, Carreau model, Cross model, power-law models, and other models. Williamson's concept of pseudoplastic fluid explained the importance of fluid dynamics. It is significant because of its practical applications in a variety of industries such as biomedical sciences, geophysics, oil and gas, chemical production, and many more. Al-Chlaihawi et al. [1] examined Newtonian and non-Newtonian fluids coupled in the natural convection of hybrid-based nanofluids on a porous enclosure with the existence of entropy generation (EG). Waqas et al. [2] studied the Cattaneo–Christov (CC) double diffusion effect and bioconvective mechanism in magnetohydrodynamic (MHD) 3D nanoparticles involving motile microorganisms by employing the variable thermal conductance and thermal diffusivity features. Rizwan et al. [3] examined the rheological analysis of metallic oxide nanomaterials comprising non-Newtonian nanofluids, as well as potential heat and mass flow properties. Abderrahmane et al. [4] evaluated the mixed convection mechanism of a power-law non-Newtonian flow of nanofluid via a detachable enclosure with a spinning cylinder subject to magnetic effects. Anwar et al. [5] researched the mathematical methods of derived magnetohydrodynamic (MHD) non-Newtonian nanofluid flowing against a nonlinearly stretched surface. Waqas et al. [6] scrutinized the consequences of non-Newtonian bio-convection Marangoni nanofluid flow towards an infinite disc with ESBHS (exponential space-based heat source).

Nanofluids are fluids that contain nanosized particles of matter. The colloidal operation of nanoparticles in a specified base fluid creates nanofluids. Nanoparticles, such as carbon nanotubes (CNTs), metal alloys, carbides, as well as oxides, are usually observed in nanofluids. Oils, ethanol glycol, and water are common as base fluids. In an era of ever-increasingly higher demands for heat energy with various uses ranging from microbiology to mechanical, the remarkable input of nanotechnology to increase the rate of temperature gradient from nearby sources has piqued the concentration of technologists and scientists. An improvement in heat quality can give an advantage over competitors, such as plasma research, microelectronic devices such as microelectronic chips in computers, nuclear power plants, space cooling systems, power production, and has prompted the examination of nanotechnology because of its multiple applications in manufacturing processes such as pharmaceutical mechanisms, microsystems, cooling in automotive vehicles, heat exchangers, washing machines, and the development of nanotechnological products

has considerably assisted. Choi [7] first proposed the melting of tiny sized particles in classical fluids.

Buongiorno (2006) [8] proposed seven slip procedures to develop the thermal conductivity influence of nanoparticles, including Brownian motion, inertia, diffusiophoresis, thermophoresis diffusion, fluid drains, the Magnus impact, and gravitational forces, and indicated that only the thermophoresis diffusion effect and Brownian motion are significant in nanofluids. Imran et al. [9] discussed second grade hybrid-based nanofluids and heat transfer rate with MHD implications of a stretchy, moveable horizontal porous plate in two-dimensional unsteady flows. Ur Rasheed et al. [10] identified the Jeffrey nanofluid flow with joule heating through a vertical direction stretchable cylinder. Waqas et al. [11] considered the convective heat transport mechanism in MHD nanofluid flowing between two rotating parallel disks. Waqas et al. [12] scrutinized the heat transformation effect and viscous dissipation in nanofluid flow via a porous stretching cylinder. Jamshed et al. [13] studied the physical conditions of the mixed (magnetohydrodynamic) convection of Ostwald-de Waele nanofluids in a vented cavity in an internal elliptic cylinder. Numerous researchers investigated nanofluids with the MHD effects and thermal radiation on different geometries [14–17] in the presence of its industrial applications. Alqaed et al. [18] examined the consequences of the non-Newtonian flow of nanofluid on pressure drop and the effect of heat transport in a capillary refrigeration system related to a pouch lithium-ion battery attached to a solar system.

For the first time, the expression "activation energy" was applied by a Swedish scientist, Svante Arrhenius, in the year 1889. The activation energy, symbolized by Ea and assessed in KJ/mol, denotes the atoms' and molecules' lowest energy required to introduce the chemical reaction. The amount of activation energy varies depending on the chemical reaction; in some cases, it is zero.

Arrhenius activation energy (AAE) as well as binary chemical processes occur in heat and mass transport and have numerous uses in chemical manufacturing, geothermal groundwater, food production, and so on. Bestman [19] wrote the first projects on Arrhenius activation energy in a binary chemical reaction. Ten other investigators, including Hsiao [20], carried out experiments on that subject for valuable viscous fluids with Arrhenius activation energy that developed the current in the current atmosphere of magnetohydrodynamics (MHD) along with other considerations on the extrusion framework to enhance the system's economic performance. Hayat et al. [21] reported the Arrhenius activation energy effect on entropy generation (EG) in a rotating 3D magnetohydrodynamic flow of nanoliquids, including a binary chemical reaction. Awais et al. [22] analyzed the non-linearly Boussinesq supposition when utilized for entropy generation in the transformation of the hyperbolic tangent flow of nanofluid versus a stretchy plate. Ali et al. [23] examined the Brownian diffusion coefficient and thermophoretic diffusion coefficient effects on moving Maxwell-based nanofluid flow with bioconvection through a Riga plate by using activation energy as well as the Cattaneo–Christov (CC) heat flux model. Milani et al. [24] discovered the connection between activation energy and encouragement in rubber sulfate vulcanization. Bhatti et al. [25] observed the consequences of Arrhenius activation energy with the chemical reaction on the flow of gyrotactic motile microorganisms in magnetically charged nanofluids on a porous surface.

"Bioconvection" is proposed as a methodology with oxytactic bacteria, wherein microorganisms swim upward. This mechanism requires a variety of microorganisms, such as those that are oxytactic, destructively gravitactic, and gyrotactic. Bioconvection mechanisms have numerous applications, including microbially enhanced oil restoration, fuel models, and sedimentary pools. These microorganisms, which are unicellular organisms, can be found in animals, human bodies, and plants bodies. As a result of the absorption of multicellular and unicellular microorganisms, microorganisms are the basis of the bioconvective method because they are much denser than blood. Furthermore, nanofluid flow with bioconvection is associated with the presence of density stratified as part of the improvement system due to the interference of motile gyrotactic microorganisms and

buoyant force comprising nanoparticles. It can be seen that the effect of nanoparticle mixtures in the presence of motile microorganisms has been considerably improved. Initially, Kuznetsov [26] examined nanofluids with bioconvection and motile microorganisms. Kuznetsov [27] specified the bioconvective nanofluid with a corresponding boundary layer flow via a horizontal plane of a gyrotactic microorganism. Alharbi et al. [28] discovered the thermal radiative effects of Williamson pseudoplastic nanofluid flow with the presence of motile gyrotactic microorganisms against the heating Riga plate for bio-fuel implementations. Imran et al. [29] studied the physical properties of the bioconvective phenomenon in MHD nanofluid flow with heat transfer via a paraboloid of revolution against a horizontal surface containing gyrotactic microorganisms. Alqarni et al. [30] observed the role of 3D bioconvection in viscoelastic MHD nanofluid flow on a stretchy surface with the occurrence of a nonlinear radiative heat transference effect and variable thermal conductance. Waqas et al. [31] examined the higher-order slip outcome in bioconvective nanofluid flow thickness on a disk surface. Waqas et al. [32] considered the influence of MHD heat transfer with Fourier's and Fick's laws in bioconvection and motile microorganism coupled-stress nanofluid flow on an inclined stretched cylinder.

Many other special problems are highlighted in the literature ([33–37]) of conceptual, numerical, and observational research on bioconvection and gyrotactic motile microorganisms and their applications.

The statistical analysis and numerical solution of 3D pseudoplastic nanofluids with bioconvection under melting heat transfer have not yet been published. This is the gap in the research we sought to fill with the analysis in our study. The novelty of the current analysis is generally focused on the effect of the melting heat transfer phenomena in bio-convectional flow of 3- dimensional Pseudoplastic nanofluid including motile microorganisms via a bidirectional stretching Riga surface. Furthermore, the thermal radiation and space-based exponential heat source impact and activation energy were considered. The numerical solution was obtained from ordinary differential equations by applying the bvp4c shooting scheme built in the computational Matlab software. The physical parameters' effect with subjective flow fields is explained with figures and tables. Furthermore, the statistical analysis of the pseudoplastic nanofluid is computed by using RSM.

2. Model Explanation of Mathematical Analysis

2.1. Flow Modeling

Here, we consider the pseudoplastic bioconvective 3D magnetohydrodynamic heat transfer nanofluid flow against a Riga plate. The Riga plate comprised moving electrodes and permanent magnets designed over a plane surface. The bidirectional surface was associated in the way of x_1 and x_2 directions with x_1x_2 plane surface at $x_3 = 0$, which is displayed in Figure 1. Furthermore, thermal radiation, exponential space-based heat source, Brownian motion and thermophoresis diffusion effects in the energy equation were also assumed. The magnetic field was utilized parallel to the direction of x_3; ignored the impressed electrical and induced electromagnetic field due to lowest magnetized Reynolds number. The Buongiorno model was used for nanofluid.

Under the above stated suppositions, the boundary layer flow equations of continuity, velocity, temperature, volumetric concentration and conservation of motile microorganisms can be expressed as [38–41]:

$$\frac{\partial u_1}{\partial x_1} + \frac{\partial u_2}{\partial x_2} + \frac{\partial u_3}{\partial x_3} = 0, \tag{1}$$

$$u_1\frac{\partial u_1}{\partial x_1} + u_2\frac{\partial u_1}{\partial x_2} + u_3\frac{\partial u_1}{\partial x_3} = \nu_f^*\frac{\partial^2 u_1}{\partial x_3^2} + \sqrt{2\nu_f^*}\Gamma\frac{\partial u_1}{\partial x_3}\frac{\partial^2 u_1}{\partial x_3^2} - \frac{\sigma^*\beta_a^2}{\rho}u_1 + \frac{\pi j_0 M_0}{8\rho}e^{\left(\frac{-\pi}{a_1}z\right)} + \frac{1}{\rho_f}\begin{bmatrix}\left(1-C_f\right)\rho_f\beta^{**}g^*(T-T_\infty) - \left(\rho_p-\rho_f\right)g^*(C-C_\infty)\\ -(N-N_\infty)g^*\gamma\left(\rho_m-\rho_f\right)\end{bmatrix}, \tag{2a}$$

The Lorentz force volume density denoted by F designed for the Riga plate is in [42]

$$\mathrm{F} = \frac{\pi j_0 M_0}{8} e^{\left(\frac{-\pi}{a_1} x_3\right)} \tag{2b}$$

Here, the magnetization is symbolized by M_0 for permanent magnets; the electrode's width and magnets are indicated by a_1; and the exterior current density in the electrodes is represented by j_0 (see Figure 1)

$$u_1 \frac{\partial u_2}{\partial x_1} + u_2 \frac{\partial u_2}{\partial x_2} + u_3 \frac{\partial u_2}{\partial x_3} = \nu_f^* \frac{\partial^2 u_2}{\partial x_3^2} + \sqrt{2\nu_f^*}\Gamma \frac{\partial u_2}{\partial x_3} \frac{\partial^2 u_2}{\partial x_3^2} - \frac{\sigma \beta_a^2}{\rho} u_2, \tag{3}$$

$$\begin{aligned} u_1 \tfrac{\partial T}{\partial x_1} + u_2 \tfrac{\partial T}{\partial x_2} + u_3 \tfrac{\partial T}{\partial x_3} &= \alpha^* \tfrac{\partial^2 T}{\partial x_3^2} - \tfrac{1}{(\rho^* c)_f} \tfrac{\partial q_a^*}{\partial x_3} + \tfrac{Q_t}{(\rho^* c)_p} (T - T_\infty) \\ &+ \chi^* \left[D_B \tfrac{\partial C}{\partial x_3} \tfrac{\partial T}{\partial x_3} + \tfrac{D_T}{T_\infty} \left(\tfrac{\partial T}{\partial x_3} \right)^2 \right] + \tfrac{Q_e (T_0 - T_\infty)}{(\rho^* c)_p} \exp\left(-n v^{-0.5} \Omega^{0.5} z\right), \end{aligned} \tag{4}$$

$$u_1 \frac{\partial C}{\partial x_1} + u_2 \frac{\partial C}{\partial x_2} + u_3 \frac{\partial C}{\partial x_3} = D_B \frac{\partial^2 C}{\partial x_3^2} + \frac{D_T}{T_\infty} \frac{\partial^2 T}{\partial x_3^2} - K r^2 (C - C_\infty) \left(\frac{T}{T_\infty} \right)^m \exp\left(\frac{-E_a}{K_1 T} \right), \tag{5}$$

$$u_1 \frac{\partial N}{\partial x_1} + u_2 \frac{\partial N}{\partial x_2} + u_3 \frac{\partial N}{\partial x_3} + \left[\frac{\partial}{\partial x_3} \left(N \frac{\partial C}{\partial x_3} \right) \right] \frac{b W_c}{(C_w - C_\infty)} = D_m \frac{\partial}{\partial x_3} \left(\frac{\partial N}{\partial x_3} \right), \tag{6}$$

In the above expressions, Equation (1) represents the continuity equation. Equations (2) and (3) show the momentum equations in u and v directions, Equation (4) highlights the temperature equation, Equation (5) signifies the concentration equation and Equation (6) displays the motile microorganism equation. The boundary constraints are:

$$\begin{cases} u_1 = a(x_1 + x_2)^n,\ u_2 = b(x_1 + x_2)^n,\ u_3 = 0, \\ -k \left(\frac{\partial T}{\partial x_3} \right)\Big|_{y=0} = \rho[\lambda^* + (T_w - T_\infty) c_s], \\ -k \frac{\partial T}{\partial x_3} = h_f (T_w - T), -D_B \frac{\partial C}{\partial x_3} = h_m (C_w - C), \\ -D_m \frac{\partial N}{\partial x_3} = h_n (N_w - N)\ at\ x_3 = 0, \\ u_1 \to 0, u_2 \to 0, T \to T_\infty, C \to C_\infty, N \to N_\infty,\ as\ x_3 \to \infty. \end{cases} \tag{7}$$

Note that (u_1, u_2, u_3) indicate velocity components, x_1, x_2, x_3 coordinate axes, kinematic viscosity is symbolized by ν_f^*, ρ for the fluid density parameter, Γ material constant of the fluid, the symbol Q_e is the exponential heat source coefficient, the thermal based-heat source coefficient noted by Q_t, Brownian motion mentioned by D_B, thermophoresis diffusion coefficient display with this notation D_T, h_f shows the heat transfer coefficient, g^* is used for gravity, $(T_\infty, C_\infty, N_\infty)$ for the ambient temperature, ambient concentration and ambient bioconvection, in that order, Stefan–Boltzmann constant symbolized by σ_a^*, microorganism density denoted by ρ_m, ρ_p for density of nanoparticles, (T, C, N) used for energy, concentration and bioconvective microorganisms, respectively, the coefficient Kr^2 for the chemical reaction rate constant, and swimming microorganisms coefficient is shown by D_m, exponential index denoted by n, thermal diffusivity parameter represented by α, nanofluid temperature represented by T_0 and concentration of nanofluid denoted by C_0, mean fluid temperature is addressed by T_m, β^{**} demonstrates the volume expansion coefficient, fitted rate constant denoted by n, chemotaxis constant identified by b, W_c illustrates the cell swimming speed, activation energy is characterized by E_a, χ^* shows the ratio between effective heat capacitance, k is for the temperature dependent thermal conductivity.

Here, the radiative heat flux is indicated by in the clarification of Roseland's approximation as represented and we obtained as follows [43]:

$$q_a^* = -\frac{4\sigma_a^*}{3m^*} \frac{\partial T^4}{\partial x_3}. \tag{8}$$

$$\frac{\partial q_a^*}{\partial x_3} = -\frac{16\sigma_a^* T_\infty^3}{3m^*} \frac{\partial^2 T}{\partial x_3^2}. \tag{9}$$

Here, m^* the rate at which incident radiation declines as depth rises is called mean absorption coefficient.

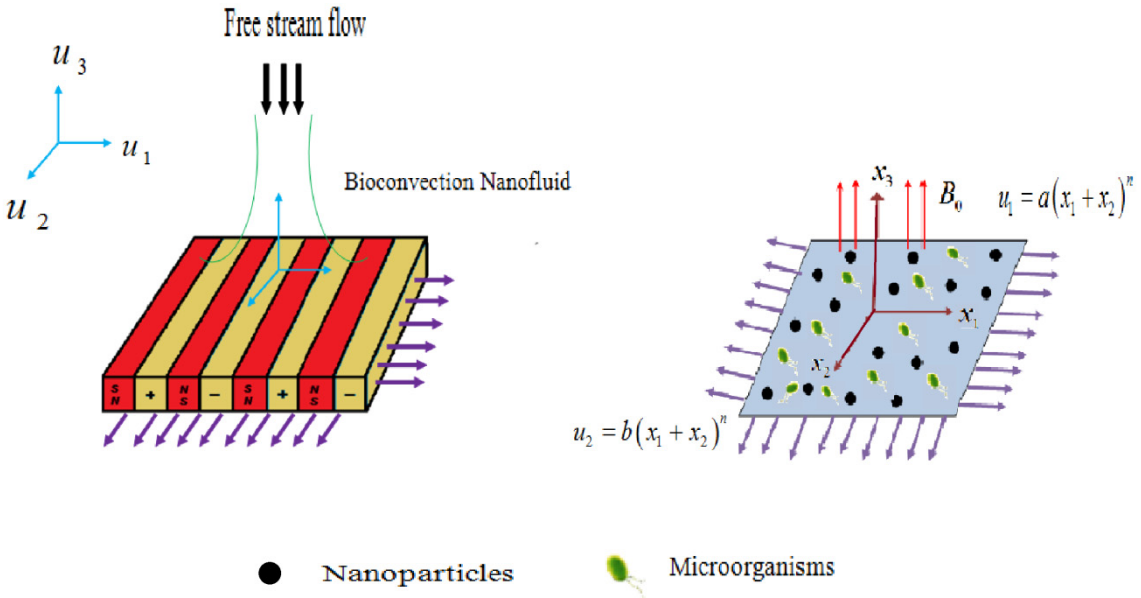

Figure 1. Geometry of the flow model.

Putting the value of q_a^* & $\frac{\partial q_a^*}{\partial x_3}$ in Equation (4) then the energy conservative Equation (10) is given below:

$$\begin{aligned} &u_1\frac{\partial T}{\partial x_1} + u_2\frac{\partial T}{\partial x_2} + u_3\frac{\partial T}{\partial x_3} = \alpha^*\frac{\partial^2 T}{\partial x_3^2} + \frac{16\sigma_a^* T_\infty^3}{3m^*(\rho^* c)_f}\frac{\partial^2 T}{\partial x_3^2} + \frac{Q_t}{(\rho^* c)_p}(T - T_\infty) \\ &+\chi^*\left[D_B\frac{\partial C}{\partial x_3}\frac{\partial T}{\partial x_3} + \frac{D_T}{T_\infty}\left(\frac{\partial T}{\partial x_3}\right)^2\right] + \frac{Q_e(T_0 - T_\infty)}{(\rho^* c)_p}\exp\left(-na^{-0.5}\nu_f^{*0.5}x_3\right), \end{aligned} \tag{10}$$

2.2. Similarity Transformation

In this section, the governing differential equation system is reduced by using the appropriate similarity transformation which is identified by the following and designated in [44,45]:

$$\begin{cases} u_1 = a\varepsilon^{\oplus} f'(\zeta),\ u_2 = b\varepsilon^{\oplus} g'(\zeta), \\ u_3 = -\sqrt{a\nu_f^*}(x_1 + x_2)^{\frac{n-1}{2}}\left(\frac{n+1}{2}(f + g) + \frac{n-1}{2}\zeta(f' + g')\right) \\ \theta(\zeta) = \frac{T - T_\infty}{T_w - T_\infty}, \phi(\zeta) = \frac{C - C_\infty}{C_\infty}, \chi(\zeta) = \frac{N - N_\infty}{N_w - N_\infty}, \\ \zeta = \sqrt{\frac{a}{\nu_f^*}}x_3(x_1 + x_2)^{\frac{n-1}{2}}, \varepsilon^{\oplus} = (x_1 + x_2)^n. \end{cases} \tag{11}$$

2.3. Resulting Reduced Equations Subjected to the Boundary Conditions

After applying the above similarity transformations, the nonlinear PDE's systems are transmuted into the following form:

$$\begin{aligned} &f''' + \left(\tfrac{n+1}{2}\right)(f' + g')f'' - n(f' + g')f' + Wef''f''' - Mf' + \beta e^{-\zeta A} \\ &+\lambda(\theta - Nr\phi - Nc\chi) = 0, \end{aligned} \tag{12}$$

$$g''' + \left(\frac{n+1}{2}\right)(f' + g')g'' - n(f' + g')g' + Weg''g''' - Mg' = 0, \tag{13}$$

$$\frac{(1+R)}{Pr}\theta'' + \left(\frac{n+1}{2}\right)(f + g)\theta' + Nb\theta'\phi' + Nt(\theta')^2 + Q_T\theta + Q_E\exp(-n\zeta) = 0, \tag{14}$$

$$\phi'' + LePr\left(\frac{n+1}{2}\right)(f+g)\phi' + \frac{Nt}{Nb}\theta'' - Le\mathrm{Pr}\sigma(1+\delta\theta)^m \exp\left(\frac{-E}{1+\delta\theta}\right)\phi = 0, \tag{15}$$

$$\chi'' + Lb\left(\frac{n+1}{2}\right)(f+g)\chi' - Pe\left[\chi'\phi' + (\Omega+\chi)\phi''\right] = 0, \tag{16}$$

The modified the reduced boundary conditions are:

$$\begin{cases} f(0) = 0, f'(0) = 1, g(0) = 0, g'(0) = \alpha, N\theta + Prf = 0, \\ \theta'(0) = -S_1(1-\theta(0)), \phi'(0) = -S_2(1-\phi(0)), \\ \chi'(0) = -S_3(1-\chi(0)) \\ f'(\infty) \to 0, g'(\infty) \to 0, \theta(\infty) \to 0, \phi(\infty) \to 0, \chi(\infty) \to 0. \end{cases} \tag{17}$$

2.4. Dimensionless Involving Parameters

The mathematical forms of the involved non-dimensional parameters are given below: Here, $Le = \frac{\alpha^*}{D_B}$ denotes the Lewis number, $Nb = \frac{\chi^* D_B C_\infty}{\nu_f^*}$ denotes the Brownian motion parameter, the mixed convection parameter is signified by $\lambda = \frac{\beta^{**} g^* (1-C_\infty)(T_w - T_\infty)}{aU_w}$, $Pr = \frac{\nu_f^*}{\alpha^*}$ designates the Prandtl number, $M = \frac{\sigma^* \beta_a^2}{\rho} a(x_1+x_2)^n$ shows the magnetic parameter, $Nt = \frac{\chi^* D_T (T_w - T_\infty)}{T_\infty \nu_f^*}$ explains the thermophoresis parameter, $R = -\frac{16\sigma_a^* T_\infty^3}{3m^*(\rho c)_f} a(x_1+x_2)^n$ demonstrates the thermal radiation parameter, the local Reynolds number is indicated by $\mathrm{Re}_x = U_w(x_1+x_2)/\nu$, $Nr = \frac{(\rho_p - \rho_f)(C_w - C_\infty)}{\rho_f(1-C_\infty)(T_w - T_\infty)\beta^{**}}$ performs the buoyancy ratio parameter, the bioconvection Rayleigh number is obtainable by $Nc = \frac{\gamma^*(\rho_m - \rho_f)(N_w - N_\infty)}{\rho_f(1-C_\infty)(T_w - T_\infty)\beta^{**}}$, $\sigma = \frac{Kr^2}{a}$ describes the chemical reaction parameter, the activation energy parameter is recognized by $E = \frac{E_a}{K_1 T_\infty}$, $Lb = \frac{\nu}{D_m}$ is the bioconvection Lewis number, Peclet number is indicated by $Pe = \frac{bW_c}{D_m}$, we display the microorganisms difference variable with $\Omega = \frac{N_\infty}{N_w - N_\infty}$, the exponential space-based heat source/sink parameter is designated by $Q_E = \frac{Q_e}{\rho c_p a}$, the thermal-based heat source/sink parameter is $Q_T = \frac{Q_t}{\rho c_p a}$, The modified Hartmann number is found with $\beta = \frac{\pi j_0 M_0}{8\rho U_w^2}$, the stretching ratio parameter suggested by $A = \frac{\pi/a_1}{a/\nu_f^*}$ for the non-dimensional parameter $\alpha = \frac{b}{a}$, thermal stratification Biot number is $S_1\left(= \frac{h_f}{k}\sqrt{\frac{\nu_f^*}{c}}\right)$, $S_2\left(= \frac{h_m}{D_B}\sqrt{\frac{\nu_f^*}{c}}\right)$ describes the solutal stratification Biot number and $S_3\left(= \frac{h_n}{D_m}\sqrt{\frac{\nu_f^*}{c}}\right)$ is designated for the microorganisms' stratification Biot number.

2.5. Physical Engineering Interest

In this section, the physical terminology properties of the local skin friction coefficient, heat transport rate, local Sherwood number and microorganism's local density number are given below:

$$\begin{aligned} &C_{fx_1} = \frac{\tau x_3 x_1}{\rho_f u_w^2}, C_{fx_2} = \frac{\tau x_3 x_2}{\rho_f v_w^2}, Nu_{x_1} = \frac{(x_1+x_2)q_w}{k(T_w - T_\infty)}, \\ &\tau x_3 x_1 = \frac{\partial u_1}{\partial x_3} + \frac{n\Gamma}{\sqrt{2}}\left(\frac{\partial u_1}{\partial x_3}\right)^2, \tau x_3 x_1 = \frac{\partial u_2}{\partial x_3} + \frac{n\Gamma}{\sqrt{2}}\left(\frac{\partial u_2}{\partial x_3}\right)^2, \\ &\mathrm{Sh}_{x_1} = \frac{(x_1+x_2)q_m}{D_B(C_w - C_\infty)}, \mathrm{Sn}_{x_1}\frac{(x_1+x_2)q_n}{D_m(N_w - N_\infty)} \end{aligned} \tag{18}$$

The reduced form of physical engineering interests are denoted as:

$$\begin{aligned} &C_f \mathrm{Re}_x^{1/2} = f''(0) + We(f'')^2(0), C_g \mathrm{Re}_x^{1/2} = g''(0) + We(g'')^2(0), \\ &\mathrm{Nu}_x \mathrm{Re}_x^{-1/2} = -\theta'(0) = (1+R)Nur, \mathrm{Sh}_x \mathrm{Re}_x^{-1/2} = -\phi'(0) = Shr, \mathrm{Sn}_x \mathrm{Re}_x^{-1/2} = -\chi'(0) = Snr. \end{aligned} \tag{19}$$

3. Numerical Scheme

In the current study, the boundary layer flow of pseudoplastic three-dimensional magnetohydrodynamic nanofluid over bidirectional stretchable Riga plate is discussed. In general the non-dimensional flow model from (12)–(16) subjected to the suitable boundary constraints (17) are solved numerically. Therefore, to find the numerical outcomes of ODEs (ordinary differential equations) through the inherent bvp4c tool in computational MATLAB software is analyzed. For this, we first converted the complicated nonlinear ODE set into first-order by using the new variables identified as follows:

$$\begin{array}{l} f = j_1, f' = j_2, f'' = j_3, f''' = j'_3, \\ g = j_4, g' = j_5, g'' = j_6, g''' = j'_6, \\ \theta = j_7, \theta' = j_8, \theta'' = j'_8, \\ \phi = j_9, \phi' = j_{10}, \phi'' = j'_{10}, \\ \chi = j_{11}, \chi' = j_{12}, \chi'' = j'_{12}, \end{array} \tag{20}$$

$$j'_3 = \frac{-\left(\frac{n+1}{2}\right)(j_2+j_5)j_3 + n(j_2+j_5)j_2 + Mj_2 - \beta e^{-\zeta A} - \Lambda^*(j_7 - Nrj_9 - Ncj_{11})}{(1+Wej_3)}, \tag{21}$$

$$j'_6 = \frac{-\left(\frac{n+1}{2}\right)(j_2+j_5)j_6 + n(j_2+j_5)j_5 + Mj_5}{(1+Wej_6)}, \tag{22}$$

$$j'_8 = \frac{-\left(\frac{n+1}{2}\right)(j_1+j_4)j_8 - Nbj_8j_{10} - Nt(j_8)^2 - Q_T j_7 - Q_E \exp(-n\zeta)}{\frac{(1+R)}{Pr}}, \tag{23}$$

$$j'_{10} = -LePr\left(\frac{n+1}{2}\right)(j_1+j_4)j_{10} - \frac{Nt}{Nb}j'_8 + Le\mathrm{Pr}\sigma(1+\delta j_7)^m \exp\left(\frac{-E}{1+\delta j_7}\right)j_9, \tag{24}$$

$$j'_{12} = -Lb\left(\frac{n+1}{2}\right)(j_1+j_4)j_{12} + Pe\left[j_{12}j_{10} + (\Omega + j_{11})j'_{10}\right], \tag{25}$$

The modified the resultant boundary conditions are:

$$\begin{cases} j_1(0) = 0, j_2(0) = 1, j_4(0) = 0, j_5(0) = \alpha, Nj_7 + Prj_1 = 0, \\ j_8(0) = -S_1(1 - j_7(0)), j_{10}(0) = -S_2(1 - j_9(0)), \\ j_{12}(0) = -S_3(1 - j_{11}(0)) \\ j_2(\infty) \to 0, j_5(\infty) \to 0, j_7(\infty) \to 0, j_9(\infty) \to 0, j_{11}(\infty) \to 0. \end{cases} \tag{26}$$

4. Results and Discussion

In this section, the melting heat transference phenomena of pseudoplastic 3D bioconvective MHD nanofluid flow against a Riga plate is examined. The numerical results were found by utilizing the MATLAB software inherent bvp4c tool. The physical properties were defined by operating the nanofluid Buongiorno model. Thermophoretic diffusion and Brownian motion effects are motivating features for fluid. Here, we found the physical descriptions of numerous parameters; for example, the magnetic parameter is M, mixed convection parameter is λ, melting parameter is N, Brownian motion parameter is Nb, buoyancy ratio parameter is Nr, bioconvection Rayleigh number is Nc, stretching parameter is α, Prandtl number is Pr, modified Hartmann number is β, thermal Biot number is S_1, solutal Biot number is S_2, thermophoresis parameter is Nt, Lewis number is Le, activation energy parameter is E, Peclet number is Pe, bioconvection Lewis number is Lb, microorganism Biot number parameter is S_3, velocity fields are f' and g', temperature profile θ, volumetric concentration field ϕ and bioconvective microorganism distribution χ are obtainable from Figures 2–24.

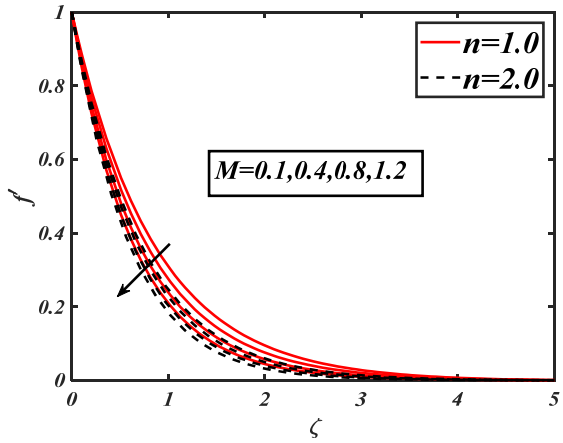

Figure 2. M illustration against f'.

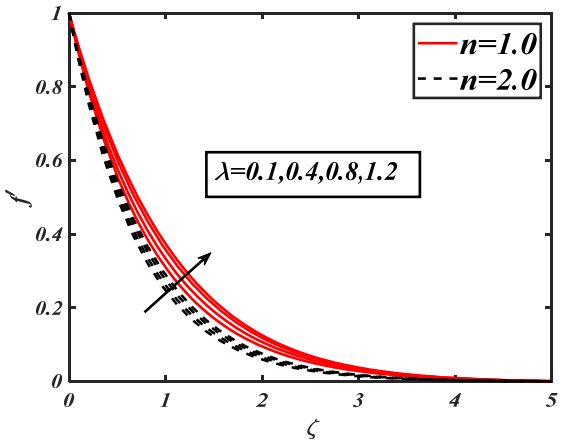

Figure 3. λ illustration against f'.

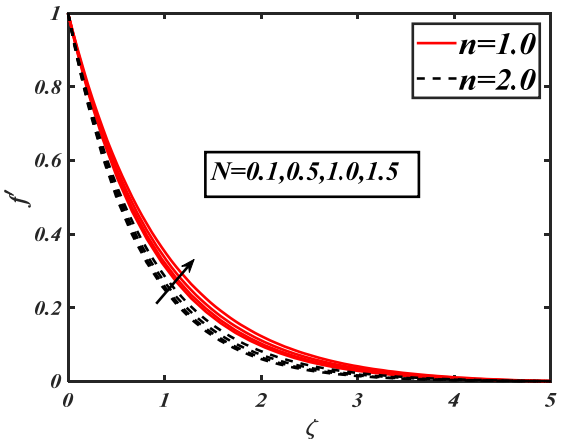

Figure 4. N illustration against f'.

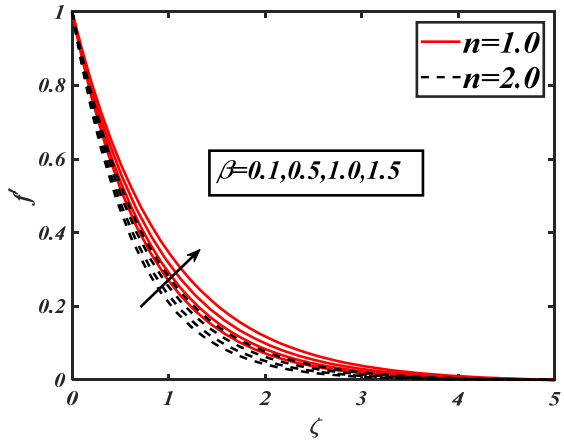

Figure 5. β illustration against f'.

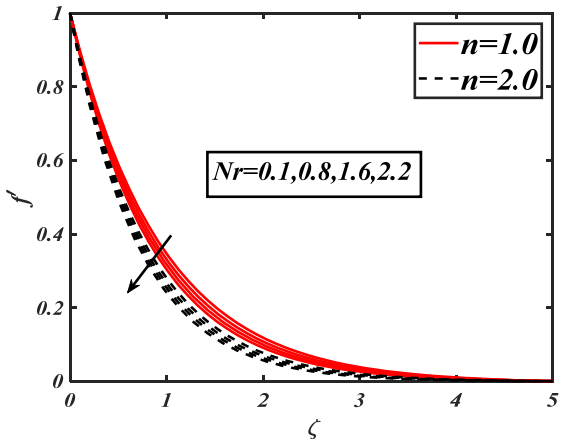

Figure 6. Nr illustration against f'.

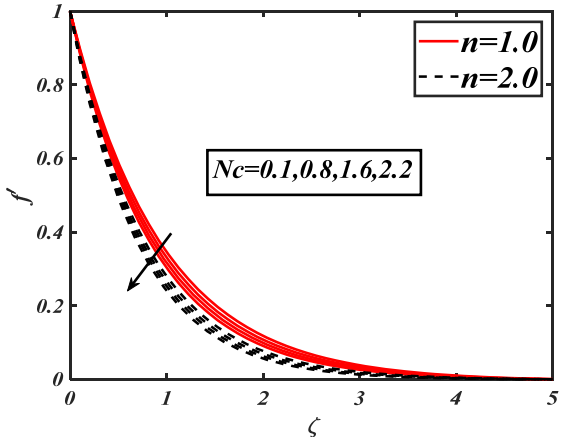

Figure 7. Nc illustration against f'.

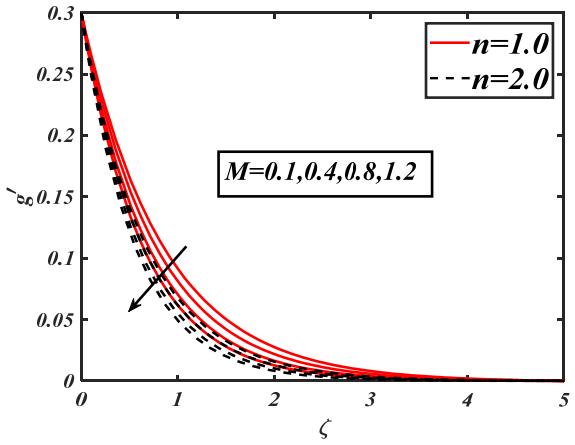

Figure 8. M illustration against g'.

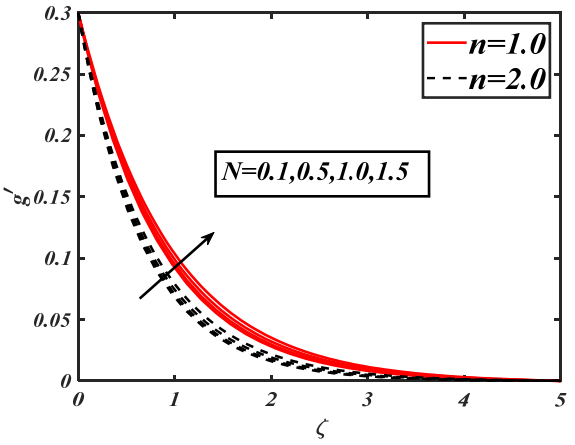

Figure 9. N illustration against g'.

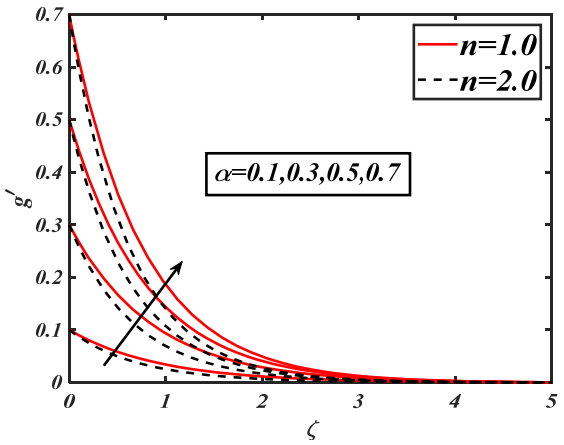

Figure 10. α illustration against g'.

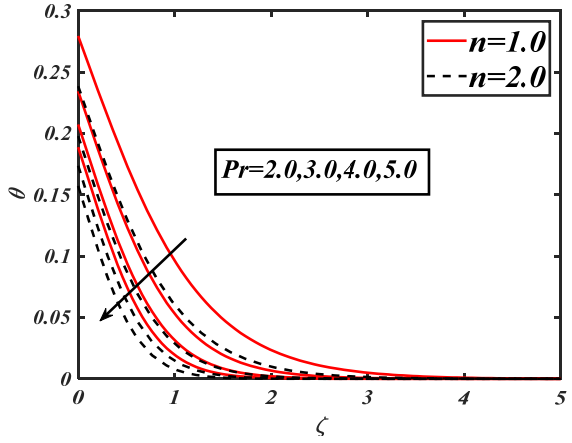

Figure 11. *Pr* illustration against θ.

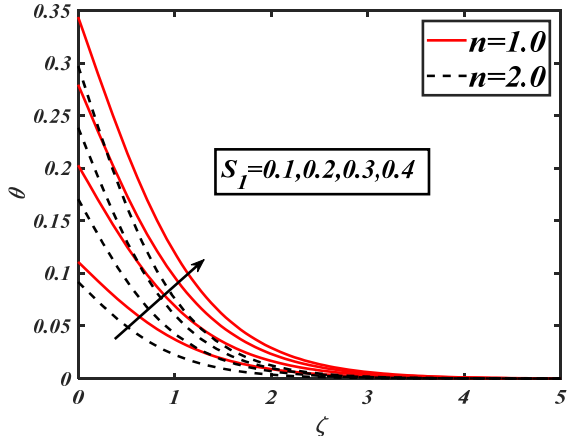

Figure 12. S_1 illustration against θ.

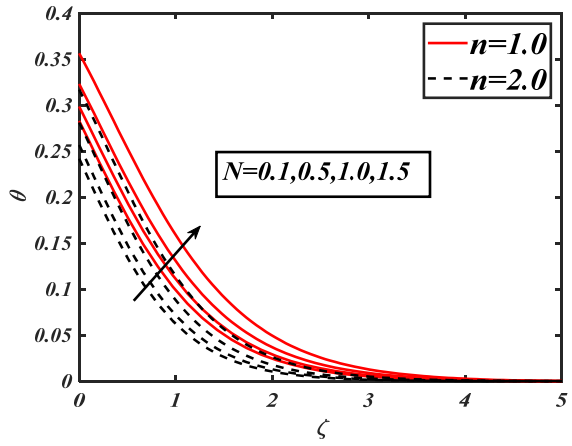

Figure 13. *N* illustration against θ.

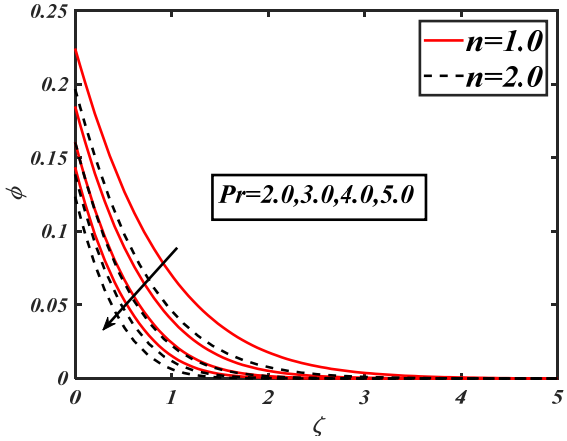

Figure 14. *Pr* illustration against ϕ.

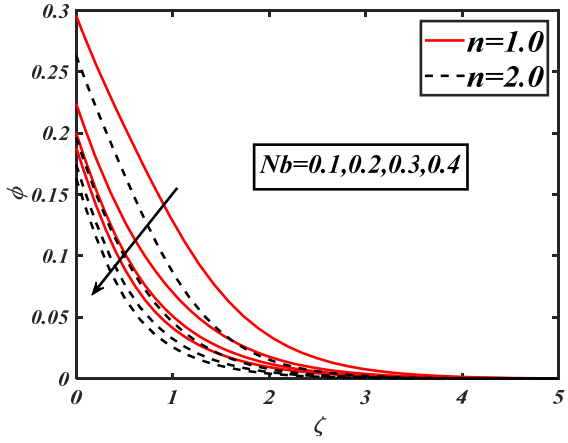

Figure 15. *Nb* illustration against ϕ.

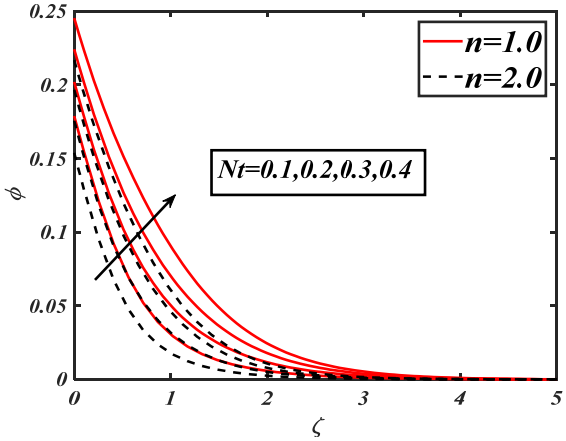

Figure 16. *Nt* illustration against ϕ.

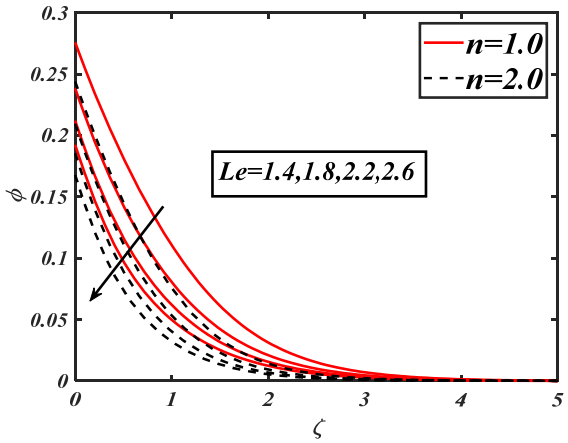

Figure 17. *Le* illustration against ϕ.

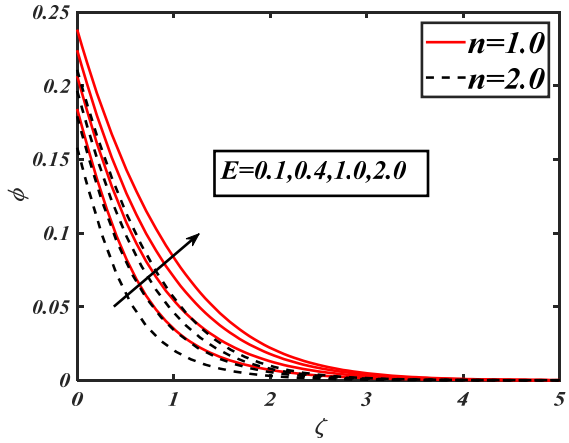

Figure 18. *E* illustration against ϕ.

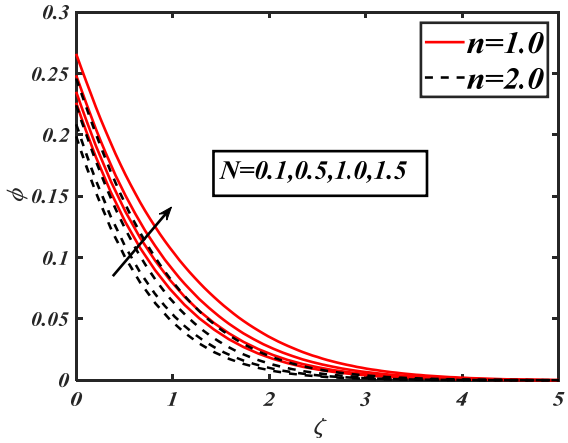

Figure 19. *N* illustration against ϕ.

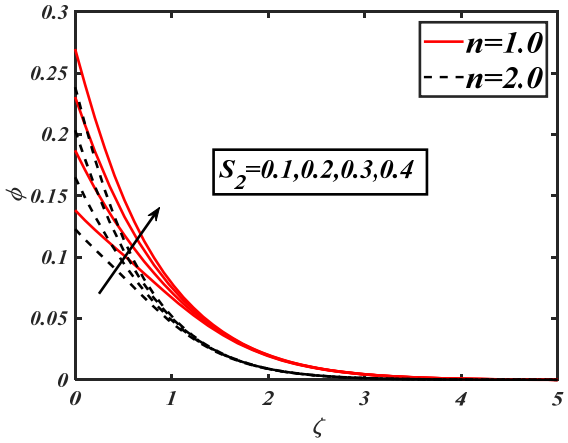

Figure 20. S_2 illustration against ϕ.

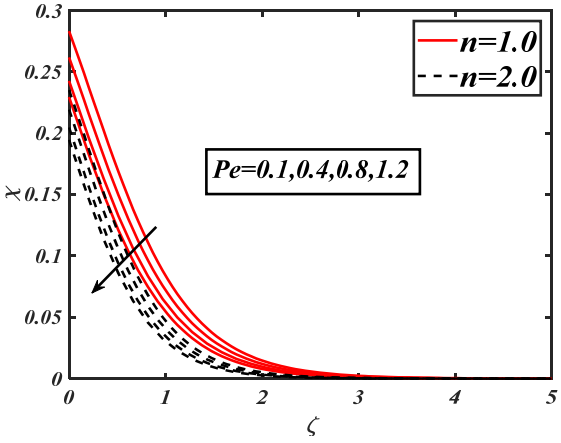

Figure 21. *Pe* illustration against χ.

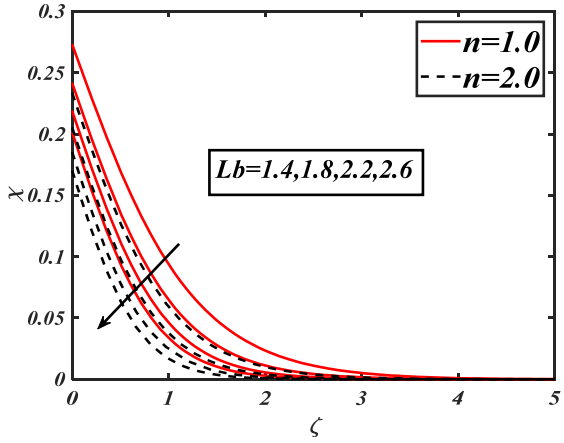

Figure 22. *Lb* illustration against χ.

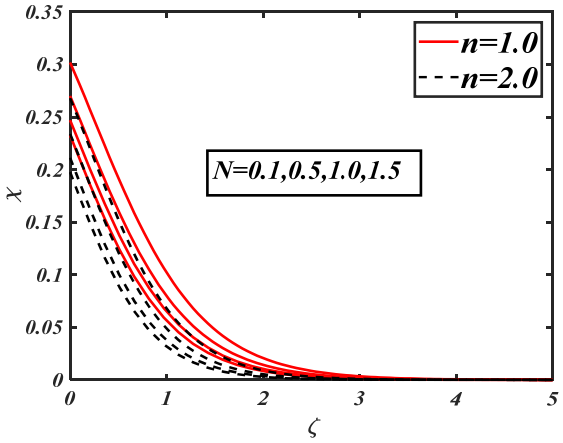

Figure 23. N illustration against χ.

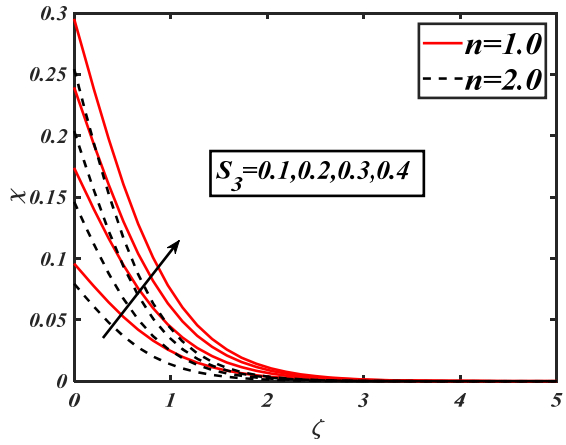

Figure 24. S_3 illustration against χ.

Figure 2 explains the magnetic parameter effect M over the flow of the fluid f'. It was found that the parameter M reduced the flow of the fluid f'. The Lorentz forces are developed due to presence of a magnetic parameter, which causes the reduction in flow of fluid f'. Figure 3 outlines the performance of mixed convection parameter λ for $n = 1$ & $n = 2$ via velocity field f'. It can be noted that the superior value of the mixed convection parameter λ enhanced the velocity field f'. Figure 4 shows the motivation of melting parameter N via the momentum field f'. Obviously, it is portrayed that the variation of melting parameter N causes increments in the velocity components f'. For conditions $n = 1$ & $n = 2$, Figure 5 shows the modified Hartmann number β over Riga plate over velocity profile f'. Commonly, the greater modified Hartmann number β reduced the flow of the fluid f'. Figure 6 presents the effect of the buoyancy ratio parameter Nr for conditions $n = 1$ & $n = 2$ over velocity field f' of the pseudoplastic nanofluid flow. The superior magnitude of the buoyancy ratio parameter Nr due to the decrease of velocity field f' can also be seen. Figure 7 illustrates the effect of the bioconvection Rayleigh number Nc versus the flow of fluid f'. It is clear that the flow of fluid f' with the conditions of $n = 1$ & $n = 2$ reduced for the incremented value of the bioconvection Rayleigh number Nc. The behavior of M over the velocity distribution g' is demonstrated in Figure 8. It is clear that the performance of the greater value of M reduced the velocity profile g'. Figure 9 shows the effect of N against velocity field g'. It was noted that the increasing variations of N boosted the velocity component g'. Figure 10 presents the values of α against the velocity profile g'. It is recognized that the raises α causes enhanced the velocity profile g' over a three-dimensional Riga plate with variable sheet thickness. Figure 11 illustrates the behavior of Prandtl number Pr for both cases $n = 1.0$ & $n = 2.0$ through temperature distri-

bution θ. It is clear that the superior Prandtl number Pr causes the temperature distribution θ to diminish. The physical effect of the Prandtl number Pr having a negative relation is experiential in the case of temperature profiles. For both conditions $n = 1.0$ and $n = 2.0$, the performance of thermal Biot number S_1 over temperature distribution θ can be described from Figure 12. Usually, it can be noted that the upsurge of the Biot number increases the thermal profile θ. Figure 13 allows scrutiny of the performance of the temperature profile via N parameter for both conditions $n = 1$ and $n = 2$. It should be noted that the larger variations of melting parameter N enlarged the thermal profile θ. Figure 14 shows the Prandtl number Pr on the solutal field of species ϕ for specific cases $n = 1.0$ & $n = 2.0$. It should be noted that for a heightened Prandtl number Pr decayed the nanoparticles solutal field of species ϕ. Figure 15 shows the significance of the Brownian motion parameter Nb against the solutal field of species. It revealed that by growing the value of the Brownian motion parameter Nb across the nanoparticles concentration profile, ϕ reduces. The performance of thermophoretic parameter Nt through the solutal field of the species of nanoparticles ϕ is given in Figure 16. An increasing behavior is noted in the solutal field of species ϕ. This arises since throughout thermophoretic effect, the smallest nanoparticles travel from the heated region towards the cold region, therefore, when the effect of thermophoresis is augmented, the heated materials transfer away from the Riga plate, causing the growth of the volumetric concentration profile. Figure 17 shows the effect of the Lewis number Le over the solutal field of species ϕ. Here, the mass concentration profile ϕ decreases due to the increasing Lewis number Le. The properties of activation energy E on the concentration field ϕ are shown in Figure 18. The concentration profile ϕ is an expanding function of activation energy E. Figure 19 exemplifies the influence of N on the volumetric concentration profile ϕ for both specific values $n = 1.0$ and $n = 2.0$. It was observed that the nanoparticle concentration field ϕ upswings for a greater value of the N parameter. The outcome of the concentration Biot number S_2 over the solutal field of species ϕ is exposed in Figure 20. It highlights that the concentration field of the nanoparticles, ϕ, improve with the growing concentration Biot number S_3.

Figure 21 represents the values in the microorganism distribution χ through an augmentation in the Peclet number Pe. Here, the microorganism profile χ reduces for greater values of the Peclet number Pe. The influence of the bioconvection Lewis number Lb against the concentration of the microorganism profile χ is shown in Figure 22. It can also be distinguished that the microorganism profile χ decays for a superior value of the bioconvection Lewis number Lb. Figure 23 considers the performance of the melting parameter N against microorganism profile χ. It was noted that a microorganism is a growing function by enhancing melting parameter N. The properties of the microorganism Biot number S_3 over microorganism distribution χ are displayed in Figure 24. The greater microorganism Biot number S_3 increased the microorganisms χ for both specific conditions $n = 1$ & $n = 2$.

In the present section, the numerical variations are described in detail. Tables 1 and 2 show that the surface drag coefficients $-f''(0)$ and $-g''(0)$ for numerous aberrations of M, λ, Nr, Nc, α, β for both cases ($n = 1.0$ and $n = 2.0$). From these present tables, scrutiny reveals that the local velocity coefficients describe an increasing trend for greater M, Nr, and Nc while they are diminished for a greater deviation of β. From Table 3, one can observe the heat transfer rate $-\theta'(0)$ versus M, λ, Nt, Pr, α, R and S_1 for both conditions ($n = 1.0$ and $n = 2.0$). The heat transport rate is a reducing function for greater values of Nt and R. Table 4 describes that the local Sherwood number upsurges due to an increase in Pr and Nb for both cases ($n = 1.0$ and $n = 2.0$). Table 5 explains that the local microorganism density number is augmented for Pe and Lb.

Table 1. Effect of flow factor over local velocity coefficient $-f''(\zeta)$ at $\zeta = 0$.

Parameters						$-f''(\zeta)$	
M	λ	Nr	Nc	α	β	n=1.0	n=2.0
0.1						**1.2129**	**1.4073**
0.3	0.1	0.1	0.1	0.3	0.1	**1.2916**	**1.4561**
0.7						**1.4364**	**1.5476**
	0.4					**1.1607**	**1.3767**
0.1	0.8					**1.1464**	**1.3696**
	1.2					**1.1322**	**1.3626**
		0.8				**1.1764**	**1.3845**
		1.4				**1.1806**	**1.3866**
		2.0				**1.1847**	**1.3887**
			0.2			**1.1763**	**1.3844**
			0.4			**1.1782**	**1.3854**
			0.8			**1.1830**	**1.3874**
				0.2		**1.1281**	**1.3347**
				0.5		**1.2934**	**1.5147**
				1.0		**1.4399**	**1.6750**
					0.2	**1.1680**	**1.3845**
					0.4	**1.1422**	**1.3612**
					0.8	**1.1233**	**1.3219**

Table 2. Effect of flow factors over velocity component $-g''(\zeta)$ at $\zeta = 0$.

Parameters						$-g''(\zeta)$	
M	λ	Nr	Nc	α	β	n=1.0	n=2.0
0.1						**0.3661**	**0.4620**
0.3	0.1	0.1	0.1	0.3	0.1	**0.3887**	**0.4788**
0.7						**0.4382**	**0.5105**
	0.4					**0.3534**	**0.4536**
0.1	0.8					**0.3541**	**0.4540**
	1.2					**0.3548**	**0.4545**
		0.8				**0.3526**	**0.4532**
		1.4				**0.3524**	**0.4531**
		2.0				**0.3522**	**0.4530**
			0.2			**0.3526**	**0.4532**
			0.4			**0.3525**	**0.4531**
			0.8			**0.3523**	**0.4530**
				0.2		**0.2266**	**0.2954**
				0.6		**0.7782**	**0.9568**
				1.0		**1.4427**	**1.6763**
					0.2	**0.3535**	**0.4322**
				0.3	0.4	**0.3499**	**0.3834**
					0.8	**0.3478**	**0.3645**

Table 3. Effect of flow factors over local Nusselt number $-\theta'(\zeta)$ at $\zeta = 0$.

Parameters							$-\theta'(\zeta)$	
M	λ	Nt	Pr	α	R	S_1	n=1.0	n=2.0
0.1							**0.0784**	**0.0805**
0.3	0.1	0.3	2.0	0.3	0.4	0.1	**0.0780**	**0.0803**
0.7							**0.778**	**0.0801**
	0.4						**0.0788**	**0.0808**
0.1	0.8						**0.0789**	**0.0809**
	1.2						**0.0790**	**0.0811**
		0.1					**0.0790**	**0.0809**
		0.5					**0.0786**	**0.0806**
		0.9					**0.0782**	**0.0804**
			2.5				**0.0805**	**0.0820**
			3.0				**0.0815**	**0.0828**
			3.5				**0.0819**	**0.0836**
				0.2			**0.0799**	**0.0805**
			2.0	0.6			**0.0798**	**0.0819**
				1.0			**0.0710**	**0.0828**
					0.6		**0.0779**	**0.0799**
				0.3	0.9		**0.0768**	**0.0789**
					1.3		**0.0756**	**0.0778**
						0.3	**0.2230**	**0.2355**
						0.6	**0.3299**	**0.3605**
						0.9	**0.3899**	**0.4344**

Table 4. Effect of flow factors over local Sherwood number $-\phi'(\zeta)$ at $\zeta = 0$.

Parameters							$-\phi'(\zeta)$	
M	λ	Nt	Pr	Nb	Le	S_2	n=1.0	n=2.0
0.1							**0.2338**	**0.2418**
0.3	0.1	0.3	2.0	0.2	2.0	0.3	**0.2332**	**0.2416**
0.7							**0.2322**	**0.2408**
	0.4						**0.2339**	**0.2418**
0.1	0.8						**0.2340**	**0.2420**
	1.2						**0.2342**	**0.2425**
		0.1					**0.2820**	**0.2968**
		0.5					**0.2585**	**0.2765**
		0.9					**0.2378**	**0.2565**
			2.5				**0.2399**	**0.2470**
			3.0				**0.2443**	**0.2508**
			3.5				**0.2476**	**0.2538**
				0.1			**0.2249**	**0.2335**
				0.5			**0.2393**	**0.2464**
				0.9			**0.2408**	**0.2478**
					3.0		**0.2444**	**0.2510**
					3.5		**0.2479**	**0.2541**
					4.0		**0.2507**	**0.2566**
						0.4	**0.3187**	**0.3111**
						0.6	**0.4111**	**0.4337**
						0.8	**0.5048**	**0.5384**

Table 5. Effect of flow factor over local density number of microorganisms $-\chi'(\zeta)$ at $\zeta = 0$.

Parameters					$-\chi'(\zeta)$	
M	λ	***Pe***	***Lb***	S_3	***n***=1.0	***n***=2.0
0.1					**0.2197**	**0.2305**
0.3	0.1	0.1	2.0	0.3	**0.2185**	**0.2299**
0.7					**0.2168**	**0.2289**
	0.4				**0.2199**	**0.2306**
0.1	0.8				**0.2205**	**0.2308**
	1.2				**0.2208**	**0.2309**
		0.4			**0.2261**	**0.2354**
		0.8			**0.2310**	**0.2391**
		1.2			**0.2350**	**0.2425**
			2.5		**0.2293**	**0.2384**
		0.1	2.8		**0.2323**	**0.2411**
			3.1		**0.2351**	**0.2435**
				0.4	**0.2743**	**0.3008**
				0.6	**0.3628**	**0.4016**
				0.8	**0.4316**	**0.4725**

The validation of the current study against the previous published work in Refs. [46,47] is shown in Table 6. The local skin friction coefficient for different values of α is reported. Here, good agreement between the current results and the published results is observed.

Table 6. Results comparison of local skin friction coefficients for several α values.

α	Ref. [46]		Ref. [47]		Present	
0.00	**1.0**	**0.0**	**1.0**	**0.0**	**1.0**	**0.0**
0.25	1.04906	0.19457	1.048811081	0.194563829	1.0488110815	0.1945638295
0.50	1.09324	0.46532	1.093095021	0.465204842	1.0930950219	0.4652048428
0.75	1.13458	0.79470	1.134485748	0.794618263	1.1344857489	0.7946182636
1.00	1.17378	1.17378	1.173720748	1.173720748	1.1737207488	1.1737207485

5. Statistical Analysis

In this section, the statistical analysis of the experimental design for three different parameters, namely, the thermophoresis parameter, the Brownian motion parameter and the Prandtl number via response. The design parameters and levels are shown in Table 7. The residual plot versus normal probability is shown in Figure 25. From the observation order observed, the residual was 0.015. From the normal probability plot, linear residuals were observed.

Table 7. Design parameters and levels.

Parameters	*Codes*	*Level*		
		Low (−1)	**Medium (0)**	**High (1)**
Nt	A_1	0.2	0.5	0.8
Nb	A_2	0.2	0.5	0.8
Pr	A_3	0.01	0.025	0.04

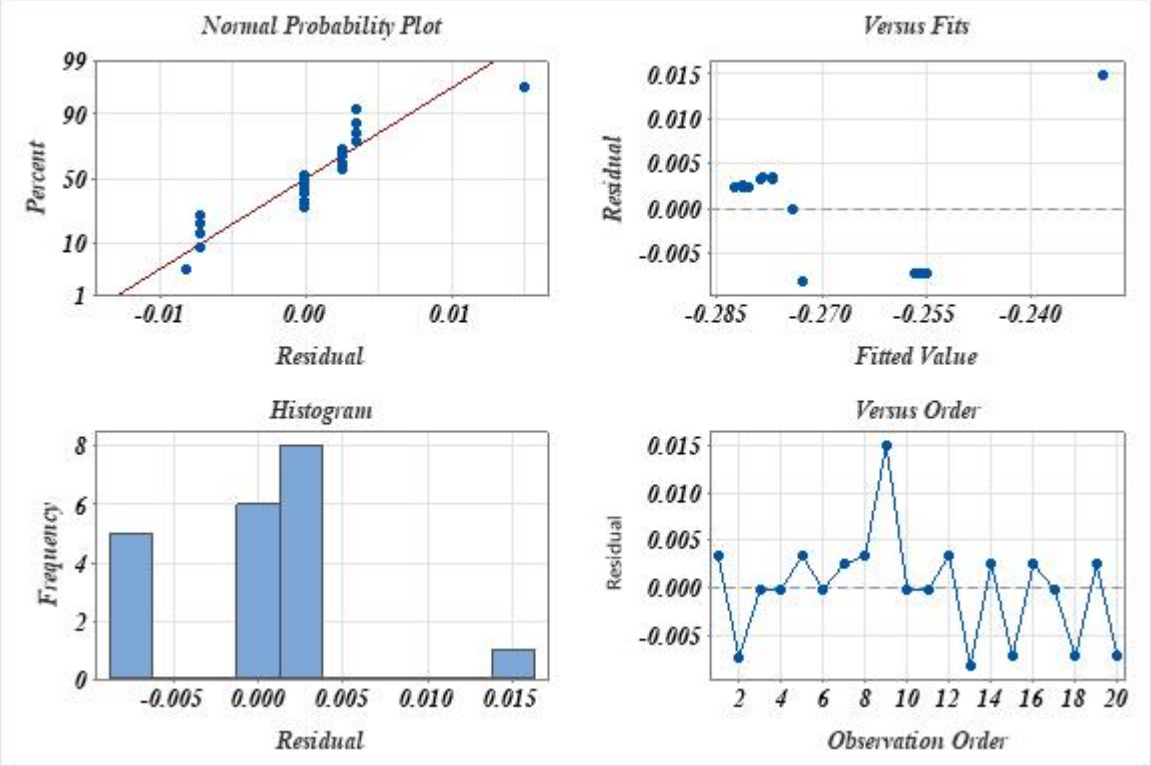

Figure 25. Plots of residual.

RSM

Response surface methodology (RSM) is a potent tool for engineering problem optimization. The strategy can be used whenever a system's efficiency is impacted by a number of different factors. Response refers to the system's performance rating when independent variables (or input variables) are changed by the operator. The main goal of this study was to use RSM to create an appropriate correlation among the input parameters and the response. Here, three factors were taken and designed for response; their lower and upper levels are also discussed.

The designed values and actual values of the experimental design factors and their response are summarized in Table 8. Here, 20 runs, coded values and their response were observed.

The analysis of variance (ANOVA) was examined to illustrate the F-value, *p*-value, Adj SS, Adj MS for the current experimental design. If the *p*-values are less than 0.05 and F-values are greater than 1, the model is significant, otherwise the model is negligible. The ANOVA results are shown in Table 9. From the variance analysis, it was observed that the model was significant. Here, the *p*-value was <0.05 and F-value was >1, which showed the model was fit.

From the analysis, the R-sq value was 85.14% and the R-sq (adj) 71.89% residuals suggested the model was fit because the difference between the R-sq and R-sq (adj) was acceptable.

The coded coefficient values are summarized in Table 10. If the *p*-value was >0.05 and F-value was <1 then the term was neglected. From the coded coefficient, the regression equation was produced and defined as:

Response = −0.2367 + 0.0280 Nt + 0.0268 Nb − 0.01690 Pr − 0.0317 Nt*Nt −0.0312 Nb*Nb + 0.001305 Pr*Pr − 0.0003 Nt*Nb + 0.00003 Nt*Pr + 0.00012 Nb*Pr

The contour plot of the design parameters versus response is shown in Figure 26. Here, the specific combination of design parameters via response was computed. The response was reduced via the thermophoresis parameter. The response for the Prandtl number was larger. The thermophoresis and Brownian motion caused the improvement in response.

Table 8. Response via coded and real values of design parameters.

Runs	*Coded Values*			*Real Values*			*Response*
	A_1	A_2	A_3	*Nt*	*Nb*	*Pr*	*Nu*
1	−1	−1	0.1	0.600000	0.200000	7.00000	−0.2789
2	1	−1	−1	0.400000	0.063641	4.50000	−0.2752
3	−1	1	−1	0.400000	0.400000	0.29552	−0.2148
4	1	1	−1	0.400000	0.400000	4.50000	−0.2745
5	−1	−1	1	0.400000	0.400000	4.50000	−0.2745
6	1	−1	1	0.736359	0.400000	4.50000	−0.2736
7	−1	1	1	0.400000	0.400000	8.70448	−0.2809
8	1	1	1	0.200000	0.600000	7.00000	−0.2789
9	−1	0	0	0.600000	0.600000	2.00000	−0.2623
10	1	0	0	0.200000	0.200000	7.00000	−0.2800
11	0	−1	0	0.400000	0.400000	4.50000	−0.2745
12	0	1	0	0.200000	0.200000	2.00000	−0.2641
13	0	0	−1	0.600000	0.600000	7.00000	−0.2779
14	0	0	1	0.200000	0.600000	2.00000	−0.2633
15	0	0	0	0.600000	0.200000	7.00000	−0.2789
16	0	0	0	0.400000	0.063641	4.50000	−0.2752
17	0	0	0	0.400000	0.400000	0.29552	−0.2148
18	0	0	0	0.400000	0.400000	4.50000	−0.2745
19	0	0	0	0.400000	0.400000	4.50000	−0.2745
20	0	0	0	0.736359	0.400000	4.50000	−0.2736

Table 9. ANOVA.

Source	**DF**	**Adj SS**	**Adj MS**	**F-Value**	***p*-Value**
Model	9	0.003298	0.000366	6.37	0.004
Linear	3	0.002225	0.000742	12.89	0.001
Nt	1	0.000004	0.000004	0.06	0.804
Nb	1	0.000003	0.000003	0.05	0.829
Pr	1	0.002219	0.002219	38.54	0.000
Square	3	0.001073	0.000358	6.21	0.012
Nt*Nt	1	0.000023	0.000023	0.40	0.540
Nb*Nb	1	0.000022	0.000022	0.39	0.546
Pr*Pr	1	0.000959	0.000959	16.65	0.002
2-Way interaction	3	0.000000	0.000000	0.00	1.000
Nt*Nb	1	0.000000	0.000000	0.00	0.996
Nt*Pr	1	0.000000	0.000000	0.00	0.996
Nb*Pr	1	0.000000	0.000000	0.00	0.982
Error	10	0.000576	0.000058		
Lack-of-fit	5	0.000576	0.000115	*	*
Pure error	5	0.000000	0.000000		
Total	19	0.003873			
R-sq	85.14%	**R-sq(adj)**	71.76%		

Table 10. Coefficients for design model.

Term	**Coef**	**SE Coef**	**T-Value**	***p*-Value**	**VIF**
Constant	−0.27431	0.00309	−88.65	0.000	
Nt	0.00052	0.00205	0.25	0.804	1.00
Nb	0.00046	0.00205	0.22	0.829	1.00
Pr	−0.01275	0.00205	−6.21	0.000	1.00
Nt*Nt	−0.00127	0.00200	−0.63	0.540	1.02
Nb*Nb	−0.00125	0.00200	−0.62	0.546	1.02
Pr*Pr	0.00816	0.00200	4.08	0.002	1.02
Nt*Nb	−0.00001	0.00268	−0.00	0.996	1.00
Nt*Pr	0.00001	0.00268	0.00	0.996	1.00
Nb*Pr	0.00006	0.00268	0.02	0.982	1.00

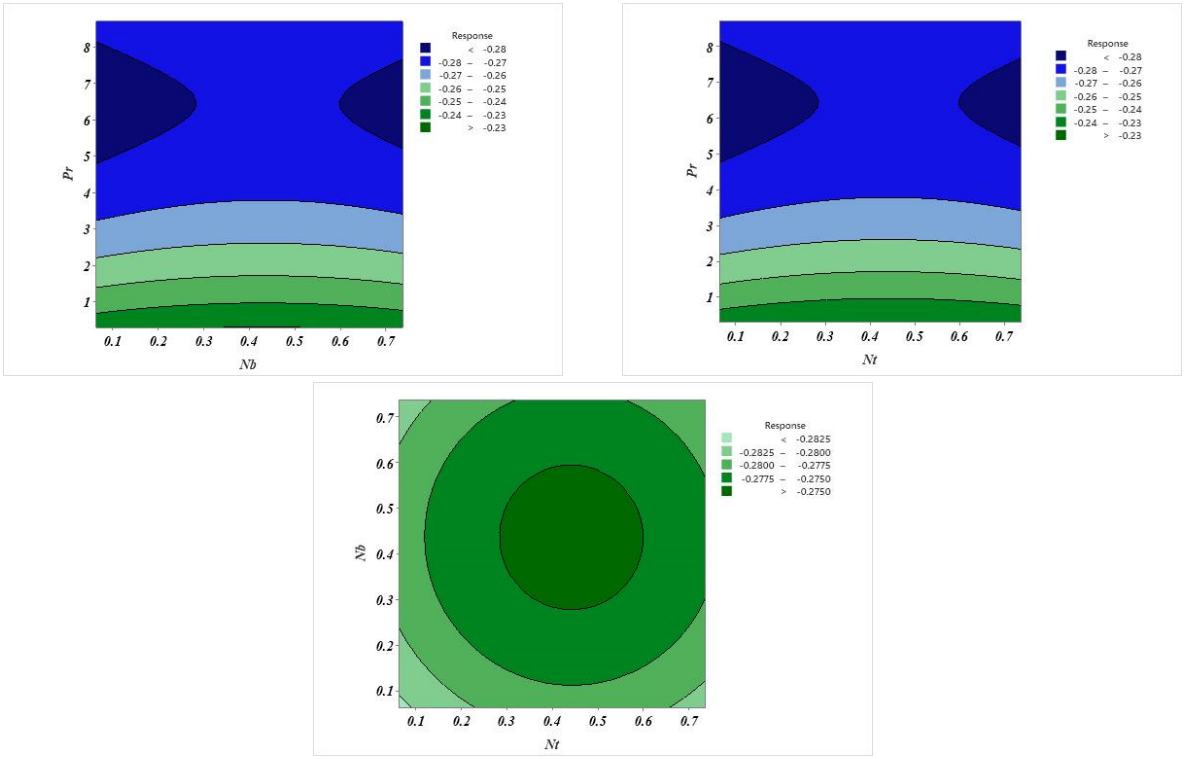

Figure 26. Contour plot.

6. Main Remarks

The main properties of pseudoplastic three-dimensional MHD heat transfer nanofluid flow with bioconvection occurrences via a Riga plate in the existence of the phenomena of melting heat transfer are revealed in this article. In addition, the Brownian motion and thermophoresis diffusion properties are also discussed in this investigation. The main important remarks of this study are noted below:

1. The greater magnitudes of the mixed convection parameter outcome in augmenting the behavior of the velocity profile.
2. Both velocity components improve for a greater melting parameter.
3. The temperature field of the nanoparticles upsurges for greater values of thermal Biot number.
4. The concentration of nanoparticles escalates for a superior thermophoresis parameter value, activation energy parameter and mass Biot number while an inverse performance is found for the Prandtl number and Lewis number.
5. The microorganism's field diminishes for a greater Peclet number and bioconvection Lewis number.
6. From the ANOVA analyzed, this model is significant.

Author Contributions: Conceptualization, H.W. and M.I.K.; methodology, S.Y. (Sumeira Yasmin); software, S.U.K.; validation, M.O. and K.G.; formal analysis, S.Y. (Song Yang); investigation, O.T.B.; resources, M.I.K.; data curation, H.W.; writing—original draft preparation, E.S.M.T.-E.; writing—review and editing, A.M.G.; visualization, A.M.G.; supervision, M.I.K.; project administration, H.W.; funding acquisition, E.S.M.T.-E. All authors have read and agreed to the published version of the manuscript.

Funding: This research was funded by Deanship of Scientific Research at Umm Al-Qura University for supporting this work by Grant Code: 22UQU4340474DSR09.

Institutional Review Board Statement: Not applicable.

Informed Consent Statement: Not applicable.

Data Availability Statement: All the data are clearly available in the manuscript.

Acknowledgments: The authors would like to thank the Deanship of Scientific Research at Umm Al-Qura University for supporting this work by Grant Code: 22UQU4340474DSR09.

Conflicts of Interest: The authors declare no conflict of interest.

Nomenclature

$(u_1$, u_2 and $u_3)$	Fluid velocity components
$(x_1$, x_2, and $x_3)$	Directions of cortisone coordinates system
M	Magnetic parameter
B_a^2	Magnetic field
$(\rho^* c)_f$	Heat capacitance of fluid
$(\rho^* c)_p$	Heat capacitance of solid particles of fluid
C_w	Concentration of wall
σ	Chemical reaction parameter
N_w	Microorganisms of wall
T_w	Wall temperature
T_∞	Ambient temperature of fluid
h_f	Heat transfer coefficient
C_∞	Ambient fluid concentration
D_B	Brownian motion
D_m	Microorganism diffusion coefficient
Nr	Buoyancy ratio parameter
N_∞	Ambient microorganisms
m^*	Mean absorption coefficient
D_T	Thermophoresis coefficient
Kr^2	Chemical reaction parameter
g^*	Gravity due to acceleration
Nc	Bio-convection Rayleigh number
R	Radiation parameter
Q_e	Exponential heat source coefficient
Q_t	Thermal-based heat source coefficient
Pr	Prandtl number
Γ	Material constant of the fluid
Nb	Brownian motion parameter
Le	Lewis number
Nt	Thermophoretic parameter
λ	Mixed convection parameter
Lb	Bioconvective Lewis number
f	Fluid velocity
β	Hartmann number
ρ_m	Microorganism density
N	Microorganism
C	Concentration of nanoparticles
Ω	Microorganism difference variable
T	Fluid temperature
ζ	Nondimensional variable
ν_f^*	Kinematic viscosity
σ^*	Electric conductivity
Pe	Peclet number
ρ	Fluid density
β^{**}	Volume expansion coefficient,
q_a^*	Radiative heat flux
M_0	Magnetization for permanent magnets
j_0	Current density
a_1	Electrode width and magnets
F	Lorentz force volume density
Re_x	Reynolds number
n	Exponential index

References

1. Al-Chlaihawi, K.K.; Alaydamee, H.H.; Faisal, A.E.; Al-Farhany, K.; Alomari, M.A. Newtonian and non-Newtonian nanofluids with entropy generation in conjugate natural convection of hybrid nanofluid-porous enclosures: A review. *Heat Transf.* **2022**, *51*, 1725–1745. [CrossRef]
2. Waqas, H.; Imran, M.; Khan, S.A.; Khan, I.; Pasha, A.A.; Irshad, K. Cattaneo–Christov double diffusion and bioconvection in magnetohydrodynamic three-dimensional nanomaterials of non-Newtonian fluid containing microorganisms with variable thermal conductivity and thermal diffusivity. *Waves Random Complex Media* **2022**, 1–20. [CrossRef]
3. Rizwan, M.; Hassan, M.; Makinde, O.D.; Bhatti, M.M.; Marin, M. Rheological modeling of metallic oxide nanoparticles containing non-newtonian nanofluids and potential investigation of heat and mass flow characteristics. *Nanomaterials* **2022**, *12*, 1237. [CrossRef]
4. Abderrahmane, A.; Alqsair, U.F.; Guedri, K.; Jamshed, W.; Nasir NA, A.; Majdi, H.S.; Marzouki, R. Analysis of mixed convection of a power-law non-Newtonian nanofluid through a vented enclosure with rotating cylinder under magnetic field. *Ann. Nucl. Energy* **2022**, *178*, 109339. [CrossRef]
5. Anwar, M.I.; Firdous, H.; Zubaidi, A.A.; Abbas, N.; Nadeem, S. Computational analysis of induced magnetohydrodynamic non-Newtonian nanofluid flow over nonlinear stretching sheet. *Prog. React. Kinet. Mech.* **2022**, *47*, 14686783211072712. [CrossRef]
6. Waqas, H.; Yasmin, S.; Khan, S.U.; Qayyum, S.; Khan, M.I.; Abbasi, A.; Sun, T.C.; Malik, M.Y. Implication of Bio-convective Marangoni flow of non-Newtonian material towards an infinite disk subject to exponential space-based heat source. *Int. J. Mod. Phys. B* **2021**, *35*, 2150252. [CrossRef]
7. Choi, S.U.; Eastman, J.A. *Enhancing Thermal Conductivity of Fluids with Nanoparticles (No. ANL/MSD/CP-84938; CONF-951135-29)*; Argonne National Lab (ANL): Argonne, IL, USA, 1995.
8. Buongiorno, J. Convective Transport in Nanofluids. *J. Heat Transf.* **2006**, *128*, 240–250. [CrossRef]
9. Imran, M.; Yasmin, S.; Waqas, H.; Khan, S.A.; Muhammad, T.; Alshammari, N.; Hamadneh, N.N.; Khan, I. Computational Analysis of Nanoparticle Shapes on Hybrid Nanofluid Flow Due to Flat Horizontal Plate via Solar Collector. *Nanomaterials* **2022**, *12*, 663.
10. Ur Rasheed, H.; AL-Zubaidi, A.; Islam, S.; Saleem, S.; Khan, Z.; Khan, W. Effects of Joule heating and viscous dissipation on magnetohydrodynamic boundary layer flow of Jeffrey nanofluid over a vertically stretching cylinder. *Coatings* **2021**, *11*, 353. [CrossRef]
11. Waqas, H.; Khan, S.A.; Muhammad, T.; Yasmin, S. Convective heat transfer in magnetized flow of nanofluids between two rotating parallel disks. *Int. J. Chem. React. Eng.* **2022**, *20*, 411–422. [CrossRef]
12. Waqas, H.; Yasmin, S.; Muhammad, T.; Imran, M. Flow and heat transfer of nanofluid over a permeable cylinder with nonlinear thermal radiation. *J. Mater. Res. Technol.* **2021**, *14*, 2579–2585. [CrossRef]
13. Jamshed, W.; Eid, M.R.; Hussain, S.M.; Abderrahmane, A.; Safdar, R.; Younis, O.; Pasha, A.A. Physical specifications of MHD mixed convective of Ostwald-de Waele nanofluids in a vented-cavity with inner elliptic cylinder. *Int. Commun. Heat Mass Transf.* **2022**, *134*, 106038. [CrossRef]
14. Mabood, F.; Muhammad, T.; Nayak, M.K.; Waqas, H.; Makinde, O.D. EMHD flow of non-Newtonian nanofluids over thin needle with Robinson's condition and Arrhenius pre-exponential factor law. *Phys. Scr.* **2020**, *95*, 115219. [CrossRef]
15. Muhammad, T.; Alamri, S.Z.; Waqas, H.; Habib, D.; Ellahi, R. Bioconvection flow of magnetized Carreau nanofluid under the influence of slip over a wedge with motile microorganisms. *J. Therm. Anal. Calorim.* **2021**, *143*, 945–957. [CrossRef]
16. Tembhare, S.P.; Barai, D.P.; Bhanvase, B.A. Performance evaluation of nanofluids in solar thermal and solar photovoltaic systems: A comprehensive review. *Renew. Sustain. Energy Rev.* **2022**, *153*, 111738. [CrossRef]
17. Riehl, R.R.; Murshed, S.S. Performance evaluation of nanofluids in loop heat pipes and oscillating heat pipes. *Int. J. Thermofluids* **2022**, *14*, 100147. [CrossRef]
18. Alqaed, S.; Mustafa, J.; Almehmadi, F.A.; Sharifpur, M. The effect of using non-Newtonian nanofluid on pressure drop and heat transfer in a capillary cooling system connected to a pouch lithium-ion battery connected to a solar system. *J. Power Sources* **2022**, *539*, 231540. [CrossRef]
19. Bestman, A.R. Natural convection boundary layer with suction and mass transfer in a porous medium. *Int. J. Eng. Res.* **1990**, *14*, 389–396.
20. Hsiao, K.L. To promote radiation electrical MHD activation energy thermal extrusion manufacturing system efciency by using Carreau-nanofuid with parameters control method. *Energy* **2017**, *130*, 486–499. [CrossRef]
21. Hayat, T.; Aziz, A.; Alsaedi, A. Analysis of entropy production and activation energy in hydromagnetic rotating flow of nanoliquid with velocity slip and convective conditions. *J. Therm. Anal. Calorim.* **2021**, *146*, 2561–2576. [CrossRef]
22. Awais, M.; Kumam, P.; Ali, A.; Shah, Z.; Alrabaiah, H. Impact of activation energy on hyperbolic tangent nanofluid with mixed convection rheology and entropy optimization. *Alex. Eng. J.* **2021**, *60*, 1123–1135. [CrossRef]
23. Ali, B.; Pattnaik, P.K.; Naqvi, R.A.; Waqas, H.; Hussain, S. Brownian motion and thermophoresis effects on bioconvection of rotating Maxwell nanofluid over a Riga plate with Arrhenius activation energy and Cattaneo-Christov heat flux theory. *Therm. Sci. Eng. Prog.* **2021**, *23*, 100863. [CrossRef]
24. Milani, G.; Milani, F. Relation between activation energy and induction in rubber sulfur vulcanization: An experimental study. *J. Appl. Polym. Sci.* **2021**, *138*, 50073. [CrossRef]

25. Bhatti, M.M.; Shahid, A.; Abbas, T.; Alamri, S.Z.; Ellahi, R. Study of activation energy on the movement of gyrotactic microorganism in a magnetized nanofluids past a porous plate. *Processes* **2021**, *8*, 328. [CrossRef]
26. Kuznetsov, A.V. Bio-thermal convection induced by two different species of microorganisms. *Int. Commun. Heat Mass Transf.* **2011**, *38*, 548–553. [CrossRef]
27. Kuznetsov, A.V. The onset of nanofluid bioconvection in a suspension containing both nanoparticles and gyrotactic microorganisms. *Int. Commun. Heat Mass Transf.* **2010**, *37*, 1421–1425. [CrossRef]
28. Alharbi, K.A.M.; Yasmin, S.; Farooq, S.; Waqas, H.; Alwetaishi, M.; Khan, S.U.; Al-Turjman, F.; Elattar, S.; Khan, M.I.; Galal, A.M. Thermal outcomes of Williamson pseudo-plastic nanofluid with microorganisms due to the heated Riga surface with bio-fuel applications. *Waves Random Complex Media* **2022**, 1–24. [CrossRef]
29. Imran, M.; Kamran, T.; Khan, S.A.; Muhammad, T.; Waqas, H. Physical attributes of bio-convection in nanofluid flow through a paraboloid of revolution on horizontal surface with motile microorganisms. *Int. Commun. Heat Mass Transf.* **2022**, *133*, 105947. [CrossRef]
30. Alqarni, M.S.; Waqas, H.; Alghamdi, M.; Muhammad, T. Importance of bioconvection in 3D viscoelastic nanofluid flow due to exponentially stretching surface with nonlinear radiative heat transfer and variable thermal conductivity. *J. Therm. Anal. Calorim.* **2022**, *147*, 4805–4819. [CrossRef]
31. Waqas, H.; Yasmin, S.; Althobaiti, N.; Bonyah, E.; Alshehri, A.; Shah, Z. Evaluating the Higher-Order Slip Consequence in Bioconvection Nanofluid Flow Configured by a Variable Thick Surface of Disk. *J. Nanomater.* **2022**, *2022*, 2766317. [CrossRef]
32. Waqas, H.; Muhammad, T.; Hussain, S.; Yasmin, S.; Rasool, G. Consequences of Fourier's and Fick's laws in bioconvective couple stress nanofluid flow configured by an inclined stretchable cylinder. *Int. J. Mod. Phys. B* **2021**, *35*, 2150176. [CrossRef]
33. Henda, M.B.; Waqas, H.; Hussain, M.; Khan, S.U.; Chammam, W.; Khan, S.A.; Tlili, I. Applications of activation energy along with thermal and exponential space-based heat source in bioconvection assessment of magnetized third grade nanofluid over stretched cylinder/sheet. *Case Stud. Therm. Eng.* **2021**, *26*, 101043. [CrossRef]
34. Chu, Y.M.; Waqas, H.; Hussain, S.; Yasmein, S.; Khan, S.U.; Khan, M.I.; Kadry, S. Joule heating, activation energy and modified diffusion analysis for 3D slip flow of tangent hyperbolic nanofluid with gyrotactic microorganisms. *Mod. Phys. Lett. B* **2021**, *35*, 2150278. [CrossRef]
35. Waqas, H.; Khan, S.A.; Khan, S.U.; Khan, M.I.; Kadry, S.; Chu, Y.M. Falkner-Skan time-dependent bioconvrction flow of cross nanofluid with nonlinear thermal radiation, activation energy and melting process. *Int. Commun. Heat Mass Transf.* **2021**, *120*, 105028. [CrossRef]
36. Abbasi, A.; Farooq, W.; Tag-ElDin, E.S.M.; Khan, S.U.; Khan, M.; Guedri, K.; Elattar, S.; Waqas, M.; Galal, A.M. Heat Transport Exploration for Hybrid Nanoparticle (Cu, Fe_3O_4)-Based Blood Flow via Tapered Complex Wavy Curved Channel with Slip Features. *Micromachines* **2022**, *13*, 1415. [CrossRef]
37. Kiranakumar, H.V.; Thejas, R.; Naveen, C.S.; Khan, M.I.; Prasanna, G.D.; Reddy, S.; Oreijah, M.; Guedri, K.; Bafakeeh, O.T.; Jameel, M. A review on electrical and gas-sensing properties of reduced graphene oxide-metal oxide nanocomposites. *Biomass Convers. Biorefinery* **2022**, *in press*. [CrossRef]
38. Dunn, J.E.; Rajagopal, K.R. Fluids of differential type: Critical review and thermodynamic analysis. *Int. J. Eng. Sci.* **1995**, *33*, 689–729. [CrossRef]
39. Khan, J.A.; Mustafa, M.; Hayat, T.; Sheikhholeslami, M.; Alsaedi, A. Three-Dimensional Flow of Nanofluid Induced by an Exponentially Stretching Sheet: An Application to Solar Energy. *PLoS ONE* **2015**, *10*, e0116603. [CrossRef]
40. Khan, M.I.; Qayyum, S.; Kadry, S.; Khan, W.A.; Abbas, S.Z. Theoretical investigations of entropy optimization in electro-magneto nonlinear mixed convective second order slip flow. *J. Magn.* **2020**, *25*, 8–14. [CrossRef]
41. Raees, A.; Raees-ul-Haq, M.; Xu, H.; Sun, Q. Tree-dimensional stagnation fow of a nanofuid containing both nanoparticles and microorganisms on a moving surface with anisotropic slip. *Appl. Math. Model.* **2016**, *40*, 4136–4150. [CrossRef]
42. Ayub, M.; Abbas, T.; Bhatti, M.M. Inspiration of slip efects on electromagnetohydrodynamics (EMHD) nanofuid fow through a horizontal Riga plate. *Eur. Phys. J. Plus* **2016**, *131*, 193. [CrossRef]
43. Alotaibi, H.; Althubiti, S.; Eid, M.R.; Mahny, K.L. Numerical treatment of MHD flow of Casson nanofluid via convectively heated non-linear extending surface with viscous dissipation and suction/injection effects. *Comput. Mater. Contin.* **2021**, *66*, 229–245. [CrossRef]
44. Ullah, M.Z.; Alshomrani, A.S.; Alghamdi, M. Significance of Arrhenius activation energy in Darcy–Forchheimer 3D rotating flow of nanofluid with radiative heat transfer. *Phys. A Stat. Mech. Its Appl.* **2020**, *550*, 124024. [CrossRef]
45. Muhammad, R.; Khan, M.I.; Jameel, M.; Khan, N.B. Fully developed Darcy-Forchheimer mixed convective flow over a curved surface with activation energy and entropy generation. *Comput. Meth. Prog. Biomed.* **2020**, *188*, 105298. [CrossRef]
46. Kumar, K.G.; Rudraswamy, N.; Gireesha, B. Effects of mass transfer on MHD three dimensional flow of a Prandtl liquid over a flat plate in the presence of chemical reaction. *Results Phys.* **2017**, *7*, 3465–3471. [CrossRef]
47. Eid, M.R. Thermal characteristics of 3D nanofluid flow over a convectively heated Riga surface in a Darcy–Forchheimer porous material with linear thermal radiation: An optimal analysis. *Arab. J. Sci. Eng.* **2020**, *45*, 9803–9814. [CrossRef]